THE JOURNAL OF CHEMICAL PHYSICS **132**, 124504 (2010)

Assessing the thermodynamic signatures of hydrophobic hydration for several common water models

Henry S. Ashbaugh,[a] Nicholas J. Collett, Harold W. Hatch, and Jennifer A. Staton
Department of Chemical and Biomolecular Engineering, Tulane University, New Orleans, Louisiana 70118, USA

(Received 16 October 2009; accepted 26 February 2010; published online 24 March 2010)

Following the conclusions of an information theory analysis that hydrophobic hydration is dictated by the equation of state of liquid water, we perform simulations of ten different water models to examine the correlation between the fidelity of each model to the experimental density of liquid water and the accuracy of its description of methane hydration. We find that the three- and five-point water models provide an inferior description of both the liquid density and methane solubility compared to the four-point water models. Of the four-point water models, TIP4P/2005 provides the best description of both the aqueous equation-of-state and methane hydration thermodynamics. When the optimized potentials for liquid simulation united-atom description for methane is used, we find that while the entropy and heat capacity of methane hydration are in excellent agreement with experiment, the chemical potential and enthalpy are systematically shifted upwards. We subsequently reoptimize the methane interaction to accurately reproduce the experimental solubilities as a function of temperature by accounting for missing attractive interactions. © *2010 American Institute of Physics*. [doi:10.1063/1.3366718]

I. INTRODUCTION

While it is reflexively understood that "oil and water do not mix," the thermodynamic puzzle of hydrophobic hydration extends beyond the meager aqueous solubility of nonpolar species to include the characteristic dependence of their solubility on temperature as well. At room temperature, the dissolution of nonpolar gases is favored by negative enthalpic contributions, but these are overwhelmed by an unfavorable negative entropy. With increasing temperature hydration eventually becomes entropically favored but soundly disfavored by a dominant positive enthalpy. The role reversal of enthalpy and entropy in opposing dissolution is indicative of a large, positive hydration heat capacity. Historically, the negative dissolution enthalpy and entropy at ambient conditions was interpreted as solute induced freezing of vicinal water molecules.[1] While providing a compelling picture, there is little experimental[2] or theoretical[3,4] evidence for an icelike hydration shell enclathrating hydrophobic moieties. Moreover, this picture does not address the heat capacity increment in a facile manner. This "iceberg" model for hydrophobic hydration has thereby become increasingly debatable over time.[5]

The hydration-free energy can be measured directly through equilibrium partitioning measurements of a solute (s) between an aqueous and vapor phase. At low pressures, the Ostwald partition coefficient, defined as

$$\frac{\rho_{\mathrm{s}}^{\mathrm{aq}}}{\rho_{\mathrm{s}}^{\mathrm{ig}}} = \exp(-\beta\mu_{\mathrm{s}}^{*}), \tag{1}$$

describes the solute distribution between an ideal gas (ig) and aqueous (aq) liquid phase. In this expression, $\rho_{\mathrm{s}}^{\alpha}$ is the density of the solute in phase α, $\beta^{-1}=kT$ is the product of Boltzmann's constant and the absolute temperature, and μ_{s}^{*} is the solute's excess chemical potential in the condensed aqueous phase.

Traditionally, the excess chemical potential of simple spherical solutes is divided between two contributions: the work associated with inserting a purely repulsive, solute-sized cavity into solution and the work of turning on attractive interactions between the solute and surrounding solvent. Based on an information theory analysis, Garde *et al.*[6,7] demonstrated the repulsive cavity contribution to the chemical potential can be modeled as

$$\mu_{\mathrm{cav}}^{*} = aT + bT\rho_{\mathrm{w}}^{2}, \tag{2}$$

where ρ_{w} is the density of water. The parameters a and b are derived from integrating the pure-water pair correlation function over the cavity volume and thereby depend on the solute radius. Empirically, however, a and b are found to be independent of temperature. Attractive contributions to the chemical potential, on the other hand, are well described following the van der Waals prescription that dispersion interactions are proportional to the solvent density,[7–9]

$$\mu_{\mathrm{vdW}}^{*} = -c\rho_{\mathrm{w}}. \tag{3}$$

The parameter c encapsulates the strength of solute-water attractive interactions, and, as for the parameters of Eq. (2), is temperature independent. For hydrophobic solutes at infinite dilution then, the total hydration-free energy is[6,7]

---

[a] Author to whom correspondence should be addressed. Electronic mail: hanka@tulane.edu.

$$\mu_s^* = \mu_{cav}^* + \mu_{vdW}^* = aT + bT\rho_w^2 - c\rho_w . \quad (4)$$

When a, b, and c are employed as fitted constants, this expression accurately captures the characteristic thermodynamic signatures of hydrophobic hydration described above,[7–10] attributing them to the unique equation-of-state properties of liquid water at ambient pressures, like the temperature of maximum density (T_{MD}) at 4 °C and its comparatively temperature insensitive isothermal compressibility.[11]

It can be argued that the equation-of-state anomalies of liquid water reflect an underlying icelike hydrogen-bond network, which in turn impact hydration and potential iceberg formation through Eq. (4).[9] However, simulation studies of the isotropic Jagla model, which exhibits a T_{MD} like water but does not form a hydrogen-bond network, reproduce the characteristics of hydrophobic solvation with no possibility of iceberg formation.[12] Similar conclusions were drawn for an isotropic model for liquid water that reproduces the room temperature pair-correlation structure of water.[13] Analytical equation-of-state studies of a waterlike model that lacks a three-dimensional network also reproduce the signatures of hydrophobic hydration.[14] One could conclude then that hydrophobic hydration is most directly influenced by water's equation of state, while solute-induced structuring potentially only plays a secondary role.[4]

In a simulation study of methane and xenon hydration in six different models for water, Paschek[9] and Krouskop *et al.*[15] found a strong correlation between hydration thermodynamics and the equation of state of each water model. Since different simulation models reproduce the experimental densities of liquid water with varying success, Paschek[9] concluded that the development of a model that accurately reproduces the liquid anomalies of water is essential for providing an accurate description of hydrophobic hydration. Since that study a number of new water models have been developed. Here, we expand Paschek's[9] original studies that considered only six different water models (three three-point models: TIP3P,[16] SPC,[17] and SPC/E;[18] two four-point models: TIP4P[16] and TIP4P/Ew;[19] and one five-point model: TIP5P[20]) to ten water models (adding three four-point models: TIP4P/Ice,[21] TIP4P/I,[22] and TIP4P/2005[23] and one five-point model: TIP5P/Ew[24]) to further explore the relationship between a model's fidelity to the liquid equation of state and its description of hydrophobic hydration.[25] Since the density anomalies of water are thought to influence hydration thermodynamics through Eq. (4), we determine the T_{MD} at atmospheric pressure for each water model and explore hydration from approximately 20 °C below to 100 °C above the density maximum. Extending beyond Paschek's[9] original studies, we extract the enthalpic, entropic, and heat capacity signatures of methane hydration at ambient conditions from the temperature dependence of the chemical potential, and use these thermodynamic quantities as an additional metric to assess the quality of the simulated water models. Based on our thermodynamic analysis, we propose a reoptimization of methane-water interactions that best captures the solubility of methane over a broad temperature range for the water model that best describes the liquid density.

II. SIMULATION DETAILS

We performed isothermal-isobaric ensemble simulations of ten popular water models at atmospheric pressure. Simulations were conducted using AMBER 9.0.[26] The water models examined include several three-point (TIP3P,[16] SPC,[17] SPC/E[18]), four-point (TIP4P,[16] TIP4P/Ew,[19] TIP4P/Ice,[21] TIP4P/I,[22] TIP4P/2005[23]), and five-point (TIP5P,[20] TIP5P/Ew[24]) water models. First, we identified the temperature at which each water model exhibits its T_{MD}. Subsequent

TABLE I. Equation-of-state properties of liquid water at atmospheric pressure. Densities are reported at 25 °C and the T_{MD}. The thermal expansion coefficient is reported at 25 °C. Thermodynamic properties were obtained by fitting liquid densities to a Laurent polynomial, $\rho_w = (\Sigma_{i=0}^5 \gamma_i T^i)/T^n$, which provides an excellent description of the isobaric density within the simulation errors (fitted parameters are listed in Table S1 of Ref. 27).

	ρ_w(25 °C) (g/cm^3)	α_w(25 °C) $\times 10^4$ (K^{-1})	T_{MD} (°C)	$\rho_w(T_{MD})$ (g/cm^3)
Experiment[a]	0.997	2.61	3.2[b]	1.000
TIP3P	0.9853 (0.0001)	8.93 (0.10)	−74.2 (1.4)	1.0388 (0.0003)
SPC	0.9772 (0.0002)	7.46 (0.10)	−51.1 (0.9)	1.0096 (0.0002)
SPC/E	0.9981 (0.0001)	5.12 (0.13)	−24.9 (0.9)	1.0129 (0.0005)
TIP4P	0.9934 (0.0001)	5.69 (0.10)	−19.2 (1.0)	1.0076 (0.0002)
TIP4P/Ew	0.9950 (0.0002)	3.41 (0.08)	−2.2 (1.0)	1.0000 (0.0002)
TIP4P/Ice	0.9929 (0.0004)	0.21 (0.17)	23.4 (1.0)	0.9929 (0.0004)
TIP4P/I	0.9964 (0.0003)	1.34 (0.11)	14.1 (1.2)	0.9974 (0.0003)
TIP4P/2005	0.9973 (0.0002)	2.93 (0.10)	2.6 (1.1)	1.0008 (0.0002)
TIP5P	0.9840 (0.0003)	4.85 (0.07)	8.0 (0.4)	0.9884 (0.0003)
TIP5P/Ew	1.0031 (0.0004)	4.79 (0.17)	7.5 (0.5)	1.0077 (0.0002)

[a] Experimental data for water from the liquid state and into the supercooled region were taken from Refs. 37 and 38, respectively. They were subsequently fit to the Laurent polynomial described in the table caption to obtain temperature derivatives.

[b] The experimental T_{MD} of water is typically reported as occurring at 4 °C rather than at 3.2 °C. We obtained this value by fitting experimental densities and solving $\alpha_w(T_{MD})=0$. Since the water density is very flat in the vicinity of the T_{MD}, however, its precise location can be sensitive to the number of points included in the Laurent polynomial fitting.

simulations were conducted from temperatures approximately 20 K below to 100 K above the T_{MD}. The melting points of most water models lie from 20 to 30 °C below the T_{MD},[21] so we may conclude that the liquid phase is stable, or only marginally supercooled, at the lowest temperatures simulated. Consecutive simulations were spaced 10 K apart, except in the vicinity of the T_{MD} where a 5 K increment was used. (The temperature ranges simulated are listed in Table S1 in the supplementary material.[27]) Between 700 and 950 water molecules were simulated. Following equilibration for at least 0.5 ns, after which the densities and internal energies fluctuate about the long-time average, an additional 10 ns simulations were performed for evaluation of thermodynamic averages. The default AMBER cutoff of 8 Å was applied to water oxygen-oxygen Lennard-Jones interactions, beyond which missing contributions were added using a continuum correction. Electrostatic interactions were evaluated using Ewald summation.[28] Berendsen's thermostat and barostat were used to control the temperature and pressure.[29,30]

Water configurations were periodically saved for postsimulation analysis of methane's chemical potential. The excess chemical potential was evaluated using Widom's test particle insertion formula[31]

$$\mu_{\mathrm{s}}^{*} = \langle \exp(-\beta\varphi_{\mathrm{sw}})\rangle_0, \tag{5}$$

where φ_{sw} is the interaction between the solute and surrounding water when the solute is randomly placed within the solvent, and the brackets, $\langle \ldots \rangle_0$, indicate averaging over solvent configurations. This average was performed by exhaustively inserting 10 000 test methanes at random positions into 50 000 saved water configurations. Methane was modeled using the optimized potentials for liquid simulation (OPLS) united-atom potential (Lennard-Jones diameter and well-depth of $\sigma_{\mathrm{ss}}=3.73$ Å and $\varepsilon_{\mathrm{ss}}=0.294$ kcal/mol, respectively).[32] Cross water-methane interaction parameters were determined by the Lorentz–Bethelot combining rules [i.e., $\sigma_{\mathrm{sw}}=(\sigma_{\mathrm{ss}}+\sigma_{\mathrm{ww}})/2$ and $\varepsilon_{\mathrm{sw}}=(\varepsilon_{\mathrm{ss}}\varepsilon_{\mathrm{ww}})^{1/2}$].[33] Direct methane-water interactions were truncated beyond a separation of 8.5 Å and supplemented with an analytical continuum correction for missing interactions.

III. RESULTS AND DISCUSSION

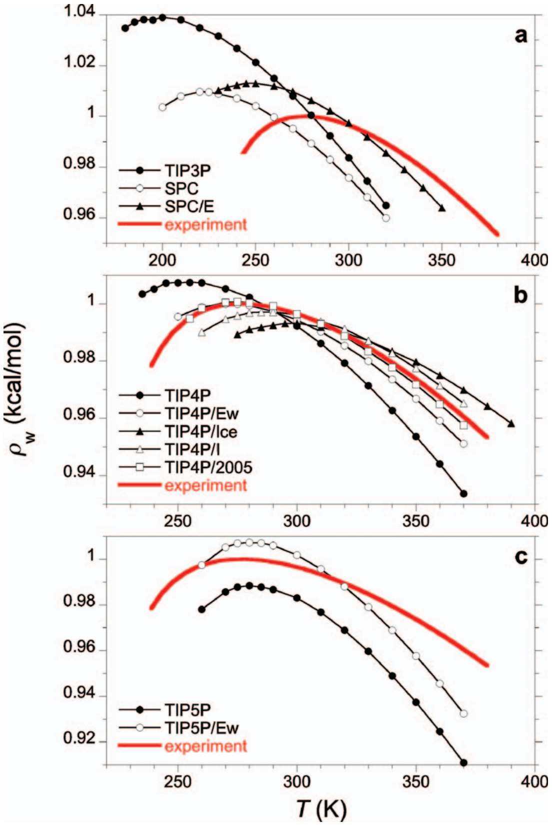

FIG. 1. Simulation density of different water models as a function of temperature at atmospheric pressure. The symbols (defined in the figure legend) indicate simulation results for the three-site (a), four-site (b), and five-site (c) water models. Simulation error bars are smaller than the symbols. The thin black lines through the simulation results are fits of the liquid densities to a Laurent polynomial function of T (functional fits are given in Table S1 in Ref. 27). The thick red experimental line indicates the density of water along the saturation curve (Ref. 38) and into the metastable supercooled regime (Ref. 39).

Based on the assumption that nonpolar solubilities are well described by Eq. (4), it follows that the potential of a water model to accurately mimic the thermodynamic signatures of hydrophobic hydration rests on its fidelity at reproducing the experimental liquid state properties of water. While the liquid densities of each water model are within 2% of the experimental value at room temperature (Table I), their temperature dependence along the one atmosphere isobar (Fig. 1) vary significantly from one water model to another. The three-point water models, for example, exhibit T_{MD}'s well below the experimental melting point of ice with densities 1%–4% greater than actually observed (Table I). The thermal expansion coefficient ($\alpha_{\mathrm{w}}=-\partial \ln \rho_{\mathrm{w}}/\partial T|_P$) of the three-point models at 25 °C are at least a factor of 2 greater than experiment (Table I), which can be anticipated to impact the hydration entropy and enthalpy through the temperature derivatives of Eq. (4),

$$s_{\mathrm{s}}^{*} = -\left.\frac{\partial \mu_{\mathrm{s}}^{*}}{\partial T}\right|_P = -a - b\rho_{\mathrm{w}}^{2}(1-2T\alpha_{\mathrm{w}}) - c\rho_{\mathrm{w}}\alpha_{\mathrm{w}} \tag{6a}$$

and

$$h_{\mathrm{s}}^{*} = \mu_{\mathrm{s}}^{*} + Ts_{\mathrm{s}}^{*} = 2bT^{2}\rho_{\mathrm{w}}^{2}\alpha_{\mathrm{w}} - c\rho_{\mathrm{w}}(1+T\alpha_{\mathrm{w}}). \tag{6b}$$

The five-point water models provide an improved description of liquid water [Fig. 1(c)], with T_{MD}'s that are only ~4 °C greater than experimentally observed (Table I). The density of TIP5P/Ew water at the T_{MD} and room temperature is in much better agreement with experiment, even over TIP5P water. The improvement of the density of TIP5P/Ew over TIP5P should not be surprising, however, since this model was optimized to work better with Ewald summation.[24] While the room temperature thermal expansion coefficients of the five-point models improve over the three-point models, they are still greater than the experimental value by nearly a factor of 2 (Table I).

The four-point models generally perform better than the three- and five-point models at reproducing the properties of water. While the original TIP4P model significantly under

TABLE II. Thermodynamic properties of methane hydration at 25 °C and atmospheric pressure. The enthalpy, entropy and heat capacity are determined by the derivatives $h_s^* = -T^2 \partial(\mu_s^*/T)/\partial T|_P$, $s_s^* = -\partial \mu_s^*/\partial T|_P$, and $c_P^* = \partial h_s^*/\partial T|_P = T\partial s_s^*/\partial T|_P$. The temperature derivatives were evaluated by fitting Eq. (4) to the simulation chemical potentials (fitted parameters are listed in Table S2 in Ref. 27).

	μ_s^* (kcal/mol)	h_s^* (kcal/mol)	s_s^* [cal/(K mol)]	c_P^* [cal/(K mol)]
Experiment	2.00	−2.72	−15.9	48.8
OPLS Methane				
TIP3P	2.12 (0.01)	0.048 (0.084)	−6.94 (0.27)	44.2 (1.9)
SPC	2.13 (0.01)	−0.59 (0.09)	−9.11 (0.28)	43.4 (3.9)
SPC/E	2.23 (0.01)	−1.30 (0.10)	−11.8 (0.3)	39.0 (3.8)
TIP4P	2.21 (0.01)	−1.14 (0.03)	−11.2 (0.1)	44.4 (2.2)
TIP4P/Ew	2.21 (0.01)	−1.93 (0.08)	−13.9 (0.3)	43.2 (3.4)
TIP4P/Ice	2.10 (0.02)	−3.46 (0.20)	−18.7 (0.6)	50.9 (6.2)
TIP4P/I	2.17 (0.01)	−2.81 (0.14)	−16.7 (0.5)	41.9 (4.6)
TIP4P/2005	2.21 (0.01)	−2.28 (0.13)	−15.0 (0.4)	47.2 (5.3)
TIP5P	1.93 (0.01)	−1.91 (0.10)	−12.9 (0.3)	76.5 (4.9)
TIP5P/Ew	1.93 (0.01)	−2.20 (0.10)	−13.8 (0.3)	78.2 (4.2)
HH-Methane				
TIP4P/Ew	2.04 (0.01)	−2.19 (0.06)	−14.2 (0.2)	41.5 (3.7)
TIP4P/I	1.97 (0.01)	−3.19 (0.20)	−17.3 (0.7)	42.7 (7.0)
TIP4P/2005	2.01 (0.01)	−2.60 (0.10)	−15.5 (0.3)	45.1 (3.8)

predicts the T_{MD} of water, TIP4P/Ew, TIP4P/I, and TIP4P/2005 all lie within ~10 °C of the experimental value. TIP4P/Ice significantly over predicts the T_{MD} of water, reflecting the fact that this model was optimized to reproduce the freezing point of water and solid phase polymorphism rather than the liquid properties.[21] Of the four-point models, TIP4P/2005 most accurately reproduces the density of water from below the freezing point to the boiling point [Fig. 1(b)]. Additionally the T_{MD} of TIP4P/2005 lies within 1 °C of the experimental value and the room temperature thermal expansion coefficient is only ~10% larger (Table I). The TIP4P/Ew and TIP4P/I water model bracket the results for TIP4P/2005. We may anticipate then that TIP4P/2005 may provide the best representation of methane solvation, followed in accuracy by the TIP4P/Ew and TIP4P/I models.

The room temperature methane hydration-free energies in differing water models lie within 10% of the experimental value (Table II), indicating that, much like the ambient density of water, solubility is not exacting enough to differentiate between models. Considering the temperature dependence of the solubility provides a more stringent test of our water and methane models. Like the density, the temperature dependence of methane's excess chemical potential varies from water model to water model (Fig. 2). Despite these differences, the aqueous chemical potentials are quantitatively described by Eq. (4), permitting evaluation of hydration enthalpies, entropies, and heat capacities after taking appropriate temperature derivatives. In general, beginning from the lowest temperatures simulated, the excess chemical potentials tend to increase with increasing temperature (Fig. 2), indicating negative hydration entropies. Moreover, these free energies have a negative concavity, indicating a positive heat capacity increment upon hydration (i.e., $c_P^* = -T\partial^2 \mu_s^*/\partial T^2|_P > 0$). The thermodynamic signatures of hydration in these different water representations are therefore qualitatively correct, although we will see below that there is significant diversity in their quantitative details.

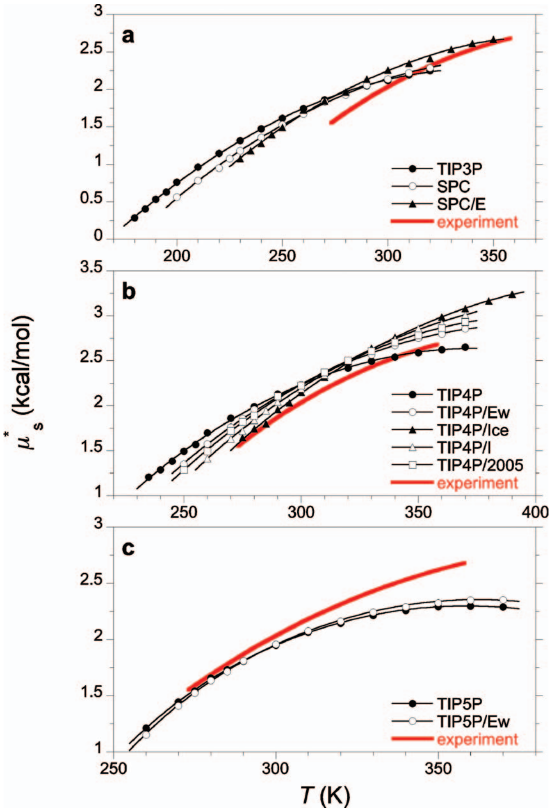

FIG. 2. Chemical potential of OPLS united-atom methane in different water models as a function of temperature. The symbols (defined in the figure legend) indicate simulation results for the three-point (a), three-point (b), and five-point (c) water models. Simulation error bars are comparable to the size of the symbols. The thin black lines indicate fits of Eq. (4) to the simulation results (functional fits are given in Table S2 in Ref. 27). The thick red experimental curve was reported in Ref. 34.

The variation of the methane hydration-free energy is stretched out over a larger temperature range than experiment for the three-point water models [Fig. 2(a)], suggesting the hydration entropies are more positive than experiment. The room temperature hydration entropies of the three-point models confirm this entropy increase (Table II). The resulting hydration enthalpy in TIP3P water at room temperature is zero within the simulation error, in marked contrast with the favorable, negative enthalpies typically associated with hydrophobic hydration. While both SPC and SPC/E perform better than TIP3P, their improvements are only marginal. The temperature dependence of the hydration enthalpy and entropy in SPC/E water is weaker than experiment, for example, having the lowest heat capacity of all the water models studied (Table II).

The room temperature hydration enthalpies and entropies of methane in the five-point water models are in improved agreement with experiment (Table II). The temperature dependence of these properties, however, is much stronger with heat capacities ~60% greater than experiment. The resulting hydration-free energies in TIP5P and

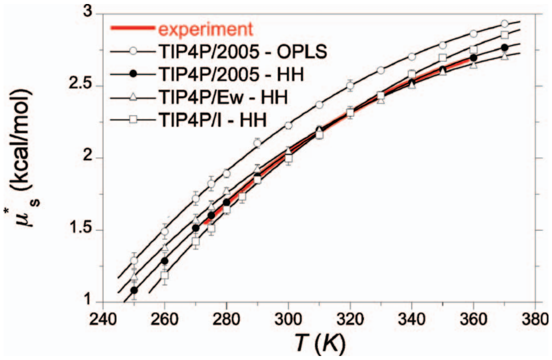

FIG. 3. Chemical potential of the reoptimized united-atom methane in as a function of temperature. The symbols (defined in the figure legend) correspond to simulation results for the OPLS united-atom methane in TIP4P/2005 water and the reoptimized hydrophobic hydration methane (HH-Methane) in TIP4P/2005, TIP4P/Ew, and TIP4P/I models. The error bars indicate one standard deviation. The thin black lines indicate fits of Eq. (4) to the simulation results (functional fits are given in Table S2 in Ref. 27). The thick red experimental curve was reported in Ref. 34.

TIP5P/Ew exhibit a maximum in the neighborhood of 355 K where the entropy crosses zero [Fig. 2(c)], compared to experimental estimates of 413 K.

As with the description of water, the hydration thermodynamic properties of methane in the four-point water models display a superior agreement with experiment than either the three- or five-point models. The progenitor TIP4P model has the poorest agreement of the four-point models [Fig. 2(b) and Table II], similar to its weaker reproduction of the water isobar. Both the room temperature hydration enthalpy and entropy of methane in TIP4P/Ice are the most negative of all the water models (Table II), potentially reflecting persistent icelike structuring that manifest in the liquid equation of state. The three remaining four-point models, TIP4P/Ew, TIP4P/I, and TIP4P/2005, have the best agreement with the room temperature thermodynamic properties (Table II), in harmony with their superior descriptions of the liquid isobar. Of these three models, the room temperature enthalpy and entropy of TIP4P/I appears to be in the best agreement with experiment. This agreement, however, worsens with changing temperature since the heat capacity of TIP4P/I is in poorer agreement with experiment than TIP4P/Ew and TIP4P/2005. The room temperature hydration-free energies of these three models are all shifted up approximately 10% from the experimental value. As can be seen Fig. 3, the hydration-free energies of methane in TIP4P/2005 water as a function of temperature are essentially parallel to experiment. Since the hydration entropy is determined by the isobaric temperature derivative of the chemical potential [Eq. (6a)], the constant shift upward for TIP4P/2005 indicates that the principal difference with the experiment results from a constant positive enthalpic shift of approximately 0.20 kcal/mol. Subtracting 0.20 kcal/mol from the room temperature enthalpies of methane in TIP4P/I and TIP4P/2005 brings TIP4P/2005 into closer agreement with experiment, while that of TIP4P/I becomes lower than experiment (Table II). While the agreement for the chemical potential and enthalpy in TIP4P/Ew improves with this shift, the enthalpy shift does not compare as well with experiment as for TIP4P/2005, and the entropy is in poorer agreement than either TIP4P/2005 or TIP4P/I.

A conclusion that can be drawn from our observations is that TIP4P/2005 provides the best description of methane hydration of all the water models studied, but that the parameterization of the united-atom OPLS methane interaction with water underestimates attractive enthalpic contributions that can lower the enthalpy. To this end, we have reoptimized the methane-TIP4P/2005 water interaction to reproduce the excess chemical potential over the available range of experimental data from 0 to 85 °C.[34] This new parameterization was achieved by varying the methane-water Lennard-Jones diameter and well-depth during test particle insertions along the water isobar to minimize the root-mean square difference between the simulation and experimental chemical potentials. The best fit cross methane-water Lennard-Jones parameters found are $\sigma_{sw}=3.470$ Å and $\varepsilon_{sw}=0.2601$ kcal/mol for a united-atom methane in TIP4P/2005 water. This reparameterization achieves a root-mean square difference of 0.007 kcal/mol over the experimental temperature range, which is comparable to the simulation error in the chemical potential (Table II). The simulation methane hydration-free energies are observed to be nearly indistinguishable from experiment (Fig. 3). The predominant change in the methane hydration thermodynamics in TIP4P/2005 at room temperature upon reoptimization is a lowering of the chemical potential and enthalpy, while the entropy and heat capacity are only marginally perturbed (Table II). The net result is a superior description of the solubility of methane in water. We refer to this reparameterized methane-water interaction as hydrophobic hydration methane (HH-Methane).

Assuming Lorentz–Bethelot combining rules, the direct methane-methane Lennard-Jones interaction for HH-Methane is $\sigma_{ss}=3.781$ Å and $\varepsilon_{ss}=0.3349$ kcal/mol. Compared to the OPLS methane parameters the Lennard-Jones diameter increases by 1.3%, while the well-depth more significantly increases by 14% in agreement with the assertion that the OPLS model largely underestimates attractive methane-water interactions. The united-atom OPLS methane interaction, which is equivalent to Siepmann's united-atom TraPPE model,[35] accurately reproduces the phase behavior of pure methane. Polarization effects are expected to be small for pure methane, since electrostatic contributions are minimal for hydrocarbons. When placed in water, however, electrostatic interactions are significant, and we attribute the increased well-depth for HH-Methane to polarization effects. Indeed, an improved description of methane solubility in TIP4P/Ew water has been recently reported when methane polarizability is taken into account.[36]

A question that naturally follows is: Is HH-Methane transferable between different water models? We have subsequently performed HH-Methane particle insertions in TIP4P/Ew and TIP4P/I water, the other two top performing water models, along their respective isobars to evaluate the chemical potential. As above, Lorentz–Berthelot combining rules were assumed to obtain cross methane-water interactions. The excess chemical potentials are shown in Fig. 3, and the calculated hydration thermodynamic properties at room temperature are given in Table II. HH-Methane solubility in both TIP4P/Ew and TIP4P/I is improved over the OPLS description, with root-mean square differences from experiment of approximately 0.04 kcal/mol apiece over the available experimental temperature range. As with their descriptions of the liquid water density, the excess chemical potentials of methane in TIP4P/Ew and TIP4P/I bracket the TIP4P/2005 and experimental results (Fig. 3), consistent with the assertion that an accurate description of the liquid equation of state of water is prerequisite for an accurate description hydrophobic hydration. While methane solubility in TIP4P/Ew and TIP4P/I could be improved by individually reoptimizing interactions for each water model, the entropy and heat capacities of methane hydration are observed to be only weakly perturbed between OPLS and HH-Methane. We believe then that optimizing methane-water interactions can only take you so far, limited by the faithfulness of the water model to experiment.

IV. CONCLUDING REMARKS

We have demonstrated from simulations of ten different water models a close correspondence between the faithfulness of each model for reproducing the liquid density at atmospheric pressure and the model's ability to account for the thermodynamic signatures of hydrophobic hydration. Of the models considered, it was found that the four-point models based on TIP4P water perform better than the three-point and five-point models. Most notably, TIP4P/2005, which provides the most realistic description of the experimental liquid density, provided the most accurate description of methane hydration. This was followed in accuracy by TIP4P/Ew and TIP4P/I. When methane is described using the united-atom OPLS model, the hydration-free energy in TIP4P/2005 is nearly parallel with the experimental results, vertically shifted up by an essentially constant value. This indicates that while OPLS methane dissolution exhibits the correct hydration entropy and heat capacity increment, it underestimates attractive enthalpic interactions between water and methane. Reoptimizing interactions, a new potential between methane and TIP4P/2005 water was developed (HH-Methane) that reproduces the thermodynamics of methane hydration over the entire range of available experimental data. When applied to the TIP4P/Ew and TIP4P/I models, HH-Methane exhibits a superior description of methane hydration than OPLS methane, although not as accurate as dissolution in TIP4P/2005 water. The main difference between HH-Methane and the OPLS model is a deeper methane-water attractive well, which we attribute to polarization effects in the aqueous environment not found in the pure hydrocarbon. This difference suggests a break down in standard Lorentz–Bethelot combining rules for transferring methane from an apolar to polar environment resulting from solute polarizability. Indeed, we anticipate a similar correction to attractive interactions for simulation models of alkanes longer than methane, which also show systematically larger vacuum-to-water transfer free energies than experiment.[37]

ACKNOWLEDGMENTS

We would like to thank Amit Jain, Ashish Sangwai, Pradeep Venkataraman, and Piyush Wanjari for assisting N.J.C., H.W.H., and J.A.S. in setting up their AMBER simulations. We also thank the two referees whose comments helped strengthen the paper. H.S.A. gratefully acknowledges financial support from the Tulane Presidential Early Career Development Award and a National Science Foundation CAREER Award (Grant No. CBET-0746955).

[1] H. S. Frank and M. E. Evans, J. Chem. Phys. **13**, 507 (1945); W. Kauzmann, Nature (London) **325**, 763 (1987).
[2] D. Laage, G. Stirnemann, and J. T. Hynes, J. Chem. Phys. **113**, 2428 (2009); P. N. Perera, K. R. Fega, C. Lawrence, E. J. Sundstrom, J. Tomlinson-Philips, and D. Ben-Amotz, Proc. Natl. Acad. Sci. U.S.A. **106**, 12230 (2009); A. Filipponi, D. T. Bowron, C. Lobban, and J. L. Finney, Phys. Rev. Lett. **79**, 1293 (1997); P. Buchanan, N. Aldlwan, A. K. Soper, J. L. Creek, and C. A. Koh, Chem. Phys. Lett. **415**, 89 (2005); D. T. Bowron, A. Filipponi, M. A. Roberts, and J. L. Finney, Phys. Rev. Lett. **81**, 4164 (1998); J. L. Finney, D. T. Bowron, R. M. Daniel, P. Timmins, and M. A. Roberts, Biophys. Chem. **105**, 391 (2003).
[3] H. S. Ashbaugh and L. R. Pratt, Rev. Mod. Phys. **78**, 159 (2006); T. Lazaridis, J. Phys. Chem. B **104**, 4964 (2000); H. S. Ashbaugh, D. Asthagiri, L. R. Pratt, and S. B. Rempe, Biophys. Chem. **105**, 323 (2003); P. J. Rossky and M. Karplus, J. Am. Chem. Soc. **101**, 1913 (1979); D. A. Zichi and P. J. Rossky, J. Chem. Phys. **84**, 2814 (1986); J. C. Owicki and H. A. Scheraga, J. Am. Chem. Soc. **99**, 7413 (1977).
[4] M. A. Gomez, L. R. Pratt, G. Hummer, and S. Garde, J. Phys. Chem. B **103**, 3520 (1999).
[5] W. Blokzijl and J. B. F. N. Engberts, Angew. Chem., Int. Ed. Engl. **32**, 1545 (1993); P. Ball, Chem. Rev. (Washington, D.C.) **108**, 74 (2008).
[6] S. Garde, G. Hummer, A. E. Garcia, M. E. Paulaitis, and L. R. Pratt, Phys. Rev. Lett. **77**, 4966 (1996).
[7] S. Garde, A. E. Garcia, L. R. Pratt, and G. Hummer, Biophys. Chem. **78**, 21 (1999).
[8] H. S. Ashbaugh and M. E. Paulaitis, Ind. Eng. Chem. Res. **45**, 5531 (2006).
[9] D. Paschek, J. Chem. Phys. **120**, 6674 (2004).
[10] D. Paschek, Phys. Rev. Lett. **94**, 217802 (2005).
[11] G. Hummer, S. Garde, A. E. Garcia, M. E. Paulaitis, and L. R. Pratt, J. Phys. Chem. B **102**, 10469 (1998); G. Hummer, S. Garde, A. E. Garcia, and L. R. Pratt, Chem. Phys. **258**, 349 (2000).
[12] S. V. Buldyrev, P. Kumar, P. G. Debenedetti, P. J. Rossky, and H. E. Stanley, Proc. Natl. Acad. Sci. U.S.A. **104**, 20177 (2007).
[13] S. Garde and H. S. Ashbaugh, J. Chem. Phys. **115**, 977 (2001).
[14] H. S. Ashbaugh, T. M. Truskett, and P. G. Debenedetti, J. Chem. Phys. **116**, 2907 (2002).
[15] P. E. Krouskop, J. D. Madura, D. Paschek, and A. Krukau, J. Chem. Phys. **124**, 016102 (2006).
[16] W. L. Jorgensen, J. Chandrasekhar, J. D. Madura, R. W. Impey, and M. L. Klein, J. Chem. Phys. **79**, 926 (1983).
[17] H. J. C. Berendsen, J. P. M. Postma, W. F. v. Gunsteren, and J. Hermans, in *Intermolecular Forces*, edited by B. Pullman (Reidel, Dordrecht, 1981), p. 331.
[18] H. J. C. Berendsen, J. R. Grigera, and T. P. Straatsma, J. Phys. Chem. **91**, 6269 (1987).
[19] H. W. Horn, W. C. Swope, J. W. Pitera, J. D. Madura, T. J. Dick, G. L. Hura, and T. Head-Gordon, J. Chem. Phys. **120**, 9665 (2004).
[20] M. W. Mahoney and W. L. Jorgensen, J. Chem. Phys. **112**, 8910 (2000).
[21] J. L. F. Abascal, E. Sanz, R. G. Fernández, and C. Vega, J. Chem. Phys. **122**, 234511 (2005).
[22] A. A. Chialvo, A. Bartók, and A. Baranyai, J. Mol. Liq. **129**, 120 (2006).
[23] J. L. F. Abascal and C. Vega, J. Chem. Phys. **123**, 234505 (2005).
[24] S. W. Rick, J. Chem. Phys. **120**, 6085 (2004).
[25] The notation *n*-point water model indicates the number of sites explicitly included to model water-water interactions. Each model has a single Lennard-Jones site center on the water oxygen. The three-point models place electrostatic charges on the water oxygen and hydrogen sites. The four-point models place positive charges on the water hydrogens and a negative charge point along the dipole, slightly ahead of the water oxy-

gen. The five-point models place positive charges on the water hydrogens and negative charges on the lone pair sites.

[26] D. A. Case, T. E. Cheatham III, T. Darden, H. Gohlke, R. Luo, K. M. Merz, Jr., A. Onufriev, C. Simmerling, B. Wang, and R. Woods, J. Comput. Chem. **26**, 1668 (2005).

[27] See supplementary material at 10.1063/1.3366718 for Tables S1 and S2, which list fits of the water density and methane chemical potentials to simulation results.

[28] S. W. de Leeuw, J. W. Perram, and E. R. Smith, Proc. R. Soc. London, Ser. A **373**, 27 (1980).

[29] H. J. C. Berendsen, J. P. M. Postma, W. F. van Gunsteren, A. DiNola, and J. R. Haak, J. Chem. Phys. **81**, 3684 (1984).

[30] Despite difficulties associated with Berendsen's weak coupling algorithm for controlling the temperature and pressure, we do not observe chemical potential differences if Andersen's thermostat is used at fixed density. We were unable to test alternate pressure control algorithms since only Berendsen's barostat has been implemented in AMBER.

[31] T. L. Beck, M. E. Paulaitis, and L. R. Pratt, *The Potential Distribution Theorem and Models of Molecular Solutions* (Cambridge University Press, Cambridge, 2006).

[32] W. L. Jorgensen, J. D. Madura, and C. J. Swenson, J. Am. Chem. Soc. **106**, 6638 (1984).

[33] M. P. Allen and D. J. Tildesley, *Computer Simulation of Liquids* (Oxford University Press, Oxford, UK, 1987).

[34] E. Wilhelm, R. Battino, and R. J. Wilcock, Chem. Rev. (Washington, D.C.) **77**, 219 (1977).

[35] M. Martin and J. Siepmann, J. Phys. Chem. B **102**, 2569 (1998).

[36] D. Paschek, Z. Phys. Chem. **223**, 1091 (2009).

[37] N. M. Garrido, A. J. Queimada, M. Jorge, E. A. Macedo, and I. J. Economou, J. Chem. Theory Comput. **5**, 2436 (2009).

[38] W. Wagner and A. Pruß, J. Phys. Chem. Ref. Data **31**, 387 (1999).

[39] D. E. Hare and C. M. Sorensen, J. Chem. Phys. **84**, 5085 (1986).